One- and two-neutron removal reactions from ^{19,20}C with a proton target

A. Ozawa *et al.*

Phys. Rev. C **84**, 064315 — Published 15 December 2011
DOI: 10.1103/PhysRevC.84.064315

One- and two-neutron removal reactions from $^{19,20}C$ with a proton target

A.Ozawa[1], Y.Hashizume[1], Y.Aoki[2], K.Tanaka[2], T.Aiba[3], N.Aoi[2], H.Baba[2], B.A.Brown[4], M.Fukuda[5], K.Inafuku[6], N.Iwasa[6], T.Izumikawa[7], K.Kobayashi[8], M.Komuro[8], Y.Kondo[9], T.Kubo[2], M.Kurokawa[2], T.Matsuyama[3], S.Michimasa[10], T.Motobayashi[2], T.Nakabayashi[9], S.Nakajima[8], T.Nakamura[9], T.Ohtsubo[3], H.Sakurai[2], R.Shinoda[8], M.Shinohara[9], H.Suzuki[2], T.Suzuki[8], M.Takechi[2], E.Takeshita[2], S.Takeuchi[2], Y.Togano[11], K.Yamada[2], T.Yamaguchi[8], T.Yasuno[1], M.Yoshitake[8]

1 Institute of Physics, University of Tsukuba, Ibaraki 305-8577, Japan

2 RIKEN Nishina-Center, Saitama 351-0198, Japan

3 Department of Physics, Niigata University, Niigata 950-2181, Japan

4 Department of Physics and Astronomy, and National Superconducting Cyclotron Laboratory, Michigan State University, Michigan 48824-1321, USA

5 Department of Physics, Osaka University, Osaka 560-0043, Japan

6 Department of Physics, Tohoku University, Miyagi 980-8578, Japan

7 Radioisotope Center, Niigata University, Niigata 951-8510, Japan

8 Department of Physics, Saitama University, Saitama 338-8570, Japan

9 Department of Physics, Tokyo Institute of Technology, Tokyo 152-8551, Japan

10 Center of Nuclear Study, University of Tokyo, Saitama 351-0198, Japan

11 Department of Physics, Rikkyo University, Tokyo 171-8501, Japan

Abstract

One and two-neutron removal-reactions from ^{19}C and ^{20}C have been studied using a liquid-hydrogen target at 40 *A* MeV. A small cross section has been observed in the one-neutron removal reaction from ^{20}C. The observed inclusive removal cross sections are compared with theoretical removal cross sections calculated by using shell model spectroscopic factors and Glauber-model single-particle cross-sections. The observed momentum distributions are also compared with those calculated by using continuum-discretized coupled-channel methods. Good consistency between theory and experiment is shown in the one-neutron removal reaction from ^{19}C. However, our theoretical calculation fails to reproduce the neutron removal reactions from ^{20}C, which suggests that further improvements of the theoretical descriptions are necessary.

PACS: 25.60.-t, 25.60.Gc; 27.20.+n; 27.30.+t
Keywords: Nuclear reactions p(^{19}C, ^{18}C), (^{20}C, ^{19}C), (^{20}C, ^{18}C), E~40 A MeV; Measured neutron removal σ; Measured longitudinal momentum distributions

1. Introduction

The invention and development of radioactive ion beams has opened a new era concerning a variety of scientific research. Investigations on the structure of exotic nuclei far from the stability line have attracted much interest in the past two decades. Among such studies, the momentum distribution of fragments is one of the most powerful tools used to investigate the structure of exotic nuclei. Via a Fourier transformation in the polar coordinate system, the momentum distribution of the fragment reflects the spatial distribution and the angular momentum of the transferred valence nucleon(s). The halo structures of ^{11}Li, ^{11}Be, ^{19}C etc. have been established through such observations [1]. Furthermore, measurements of the momentum distribution are used to investigate the configuration of the valence nucleon(s) for unstable nuclei [2].

Carbon isotopes are interesting for studying their nuclear structure, since they have a long isotope chain (A=9 to A=22). Since some nuclei in C isotopes (^{15,17,19}C) have relatively small one-neutron separation energies (S_{1n}), the halo structure for the nuclei has been investigated. Interaction cross sections (σ_I), which are defined as the sum of reaction cross section for the change of proton and/or neutron number in the incident nucleus, have been measured at relativistic energies (around 950 A MeV) for $^{9\text{-}20}$C [3]. Data show that the nuclear radii greatly increase at ^{16}C, but not at ^{15}C, where a valence neutron is located in a new shell. Although the radius of ^{19}C is much larger than those of neighbors, the radius of ^{17}C shows no enhancement. Systematic measurements of longitudinal momentum distributions ($p_{//}$) of fragments for C isotopes, up to A=19, have been made at GANIL [4] and at RIKEN [5-8]. Especially, at RIKEN, $p_{//}$ for two-neutron removal reactions have been simultaneously investigated for $^{15\text{-}19}$C isotopes. The total reaction cross sections (σ_R), which are defined by σ_I plus inelastic scattering cross sections, have been measured for $^{15\text{-}18}$C with a C target at around 80 A MeV [5,7,8] and for $^{18\text{-}22}$C with a proton target at around 40 A MeV [9,10]. σ_R of $^{18\text{-}22}$C have been successfully analyzed by Glauber model [9,10]. σ_R of ^{22}C shows that a large neutron halo structure is suggested for the nuclei [9]. Theoretical calculations based on the Glauber model for σ_R in C-isotopes have been investigated in Ref. [11,12]. The $p_{//}$ distributions for one and two-neutron removal reactions for $^{15\text{-}19}$C with a C target have been theoretically investigated using an eikonal reaction model [13].

The nuclear structure of ^{20}C is interesting, since it may have N=14 sub-shell closure.

Although N=14 sub-shell closure is suggested for oxygen isotopes [14,15], in-beam γ-ray spectroscopy performed at GANIL has shown a disappearance of the N=14 sub-shell closure in ^{20}C [16]. Inelastic scatterings on ^{208}Pb and liquid-hydrogen targets have been investigated up to ^{20}C [17]. The data show the need for a factor of about 0.4 decrease of the normal polarization charges from a simple shell-model calculation. This suggests a large decoupling of the valence neutrons from the core. Thus, the nuclear structure of the ground state of ^{20}C is still quite unknown. Since $p_{//}$ of fragments from ^{20}C is sensitive to the valence neutron(s) configuration of the ^{20}C ground state, the measurements may give a new knowledge for the nucleus.

From an experimental point of view, a liquid and/or solid hydrogen target is attractive, since the number of atoms per unit mass is the maximum. Thus, the small intensity of RI beams can be partly compensated. It is noted that, recently, transverse momentum distributions ($p_{\perp}$) of fragments from ^{18,19}C with a proton target have been measured [18]. To interpret the nuclear structure for the nuclei, the authors successfully used continuum-discretized coupled-channel (CDCC) methods [19]. CDCC analysis might be also adequate to interpret $p_{//}$. We developed our CDCC analysis code, namely HCTAK [20], and used the program to analyze the $p_{//}$ experimental data.

In the present work, we studied one- and two-neutron removal reactions from ^{19}C and ^{20}C using a liquid-hydrogen target at 40 A MeV. In section 2, we describe the experimental results along with a description of the experimental setup. In section 3, we present our analysis methods, and give discussions. We summarize the paper in section 4.

2. Experiment and results

The experiment was performed at the RIken Projectile fragment Separator (RIPS) [21], a part of the RI Beam Factory operated by RIKEN Nishina Center and CNS, the University of Tokyo. The experimental setup is shown in Fig. 1, which is essentially the same as that described in Ref. [9,10]. Secondary beams of ^{19}C and ^{20}C were produced by projectile fragmentation of the primary beam, ^{40}Ar, at 63 A MeV. The production target was Ta with a 333 mg/cm^2 thickness. At the first focus (F1) of RIPS, we used a wedge-shaped degrader and a Parallel Plate Avalanche Counter (PPAC) [22] to determine the beam position. At the second focus (F2), we used a plastic scintillator to give a start signal for a time-of-flight (TOF) measurement. The reaction target was made of liquid hydrogen (t=204 mg/cm^2), a part of the cryogenic proton and alpha target system (CRYPTA) [23], and was placed at the achromatic focus (F3). Before the reaction target, three PPACs were used to track incident nuclei and to obtain the beam position and the incident angle on the target. Particles before the reaction target were identified by the energy loss (ΔE) in two Si detectors, the TOF between two plastic scintillators located at F2 and at F3, and the magnetic rigidity. A stack of 160 NaI(Tl) crystals, called DALI2 [24], surrounded the target to detect any de-excitation γ-rays emitted from the fragments.

After the reaction target, particles were transported by a superconducting triplet quadrupole magnet (STQ) [25] to F4. We used STQ to increase the transmission efficiency from the reaction target to detectors used for particle identification. STQ also allowed us to measure TOF between F3 and F4 [26]. At F4, a plastic scintillator was used to give a stop signal of TOF. Si detectors and a NaI(Tl) detector were used to measure ΔE, and the total energy (E), respectively. Particles after the reaction target were identified by the TOF-ΔE-E method. A typical mass identification spectrum after the reaction target for the ^{20}C projectile is shown in Fig. 2, where Z=6 was selected by ΔE in the Si detectors at F4. A peak for the ^{18}C fragment is clearly shown. On the other hand, the yield of the ^{19}C fragment is quite small. This indicates that a two-neutron removal channel is dominant in the breakup of the ^{20}C projectile.

The $p_{//}$ of the fragments were obtained from the TOF measured between two plastic scintillators installed at F3 and F4. The transport of fragments between these two scintillators was made only by focusing STQ, as shown in Fig. 1. The position information from PPAC at F1 was used to derive the momentum of incident fragments. The reactions of the projectiles (^{19}C and ^{20}C) in NaI(Tl) contributed to the main source of background for the TOF spectra. The background-subtraction procedure was almost the same as described in Ref. [5]. The reaction events of the projectiles in NaI(Tl) are observed as the tail of the energy spectra in NaI(Tl), as shown in Fig. 2, where the linear function was assumed for the tail. This function has been determined by the fitting of the tail (below -200 in the mass spectra in Fig. 2). We assumed that the shape of the TOF spectrum for the background events was the same as that of the projectile. The TOF spectrum of the projectile multiplied by the scaling-down factor, which was obtained by comparing the events of the projectile with the background events of the fragments, was subtracted from the raw TOF spectra of the fragments. Then, the corrected TOF spectra were converted to the momentum. The momentum of a fragment relative to the incident projectile in the laboratory frame was transformed into that in the projectile rest frame using the relativistic kinematics. Since the magnetic fields of STQ were optimized for non-reacted events to measure σ_R at the same time, the acceptance for the fragments was simulated by the code MOCADI [26]. Calculated transmissions of the fragments in the (^{19}C, ^{18}C) reaction, the (^{20}C, ^{19}C) reaction and the (^{20}C, ^{18}C) reaction were 92 %, 94 % and 63 %, respectively. We assumed 10 % errors for the calculated transmission [5]. Our analysis indicates that a transmission correction had a very small effect on the shape of the momentum distribution.

The Lorentz-transformed $p_{//}$ of one-neutron removal reactions from ^{19}C at 40 A MeV is shown in Fig. 3-(a). Here, $p_{//}$=0 MeV/c corresponds to the momentum of ^{18}C with the same velocity of the incident ^{19}C projectile. The error indicated in the figures includes a statistical error as well as an error arising from background subtraction. A Lorentzian function was used to fit the distributions. The FWHM was determined to be 83±12 MeV/c after unfolding a Gaussian-shaped experimental system resolution of 18±1 MeV/c in σ for the ^{19}C projectile. Using the estimated transmission, the one-neutron removal cross section (σ_{-1n}) for the ^{19}C projectile (the cross section of the (^{19}C, ^{18}C) reaction) was obtained to be 101±11 mb, which is consistent with the experimental data (106±16 mb) measured at 68 A MeV [18]. The errors from the transmission estimations are included besides the statistical one. It is noted that the observed σ_{-1n} with the proton target is also consistent with σ_{-1n} with a Be target (220±65 mb) at 64 A MeV [6] if we scaled the cross section by $\sigma_{-1n} \propto (A_T^{1/3}+A_P^{1/3})^2$, where A_T (A_P) is the mass number of a target (projectile) nucleus, respectively. The observed FWHM is broader than that previously observed with a Be target (61±5 MeV/c in FWHM) [6]. This difference suggests that the reaction mechanism should be taken into account properly in the case with a proton target. Thus, the analysis of $p_{//}$ by the CDCC method was anticipated.

The $p_{//}$ distributions of one and two-neutron removal reactions in ^{20}C at 40 A MeV are shown in Fig. 4. The error bars in the figures include a statistical error as well as an error arising from background subtraction. A Lorentzian function was used to fit the distributions. The FWHMs were determined to be 168±20 MeV/c for the (^{20}C,

^{19}C) reaction and 233±39 MeV/c for the (^{20}C, ^{18}C) reaction, after unfolding the Gaussian-shaped experimental system resolution of 23±1 MeV/c in σ for the ^{20}C projectile. Using the estimated transmission value, the one- and two-neutron removal cross sections (σ_{-1n} and σ_{-2n}) from ^{20}C were obtained to be 22±8 mb and 107±15 mb, respectively. The errors from the transmission estimations are included besides the statistical one. It is noted that we did not observe any prominent peak of γ-rays if we selected ^{20}C before injecting to the hydrogen target.

3. Analysis and discussions

3-1. One neutron removal reactions

The theoretical model cross sections for one-nucleon removal to each final state, of spin-parity J^π, are calculated using

$$\sigma_{-1n} = \sum_{nlj} \left[\frac{A}{A-1} \right]^N C^2S(J^\pi, nlj)\sigma_{sp}(nlj, S_N^{eff}), \qquad (1)$$

where the C^2S are the shell model spectroscopic factors and σ_{sp} is the single-particle cross section calculated using the eikonal model assuming unit spectroscopic factor [13]. The quantum numbers of the removed neutron are denoted by *nlj* and S_N^{eff} is the effective separation energy of the neutron for N the given final state. The single-particle cross-sections (σ_{sp}) is assumed to be given by $\sigma_{tra}+\sigma_{diff}$, where σ_{tra} is the contribution of proton transfer ((p, d) reaction) and σ_{diff} is that of diffractive dissociation (elastic breakup). Shell model calculations were used for the relevant level energies and spectroscopic factors. These were performed using the code OXBASH [28]. The calculations used the WBP effective interaction [29], and a model space truncated to allow $0\hbar\omega$ and $1\hbar\omega$ excitations relative to the *p*-*sd* ground state. The small center-of-mass correction factor $[A/(A-1)]^N$, shown in Eq. (1), with N the principal oscillator model quantum number of the removed-nucleon shell, was applied to the shell model spectroscopic factors in all single-neutron removal calculations (N=1 or 2 in the present calculations). The calculated results of the level energies (E_x) and C^2S are shown in Table 1. Total reaction cross section of σ_{tra} was calculated by using zero-range distorted wave born approximation code DWUCK4 [30]. In these distorted wave calculations, the optical model parameters (OMP) for p+^{A}C were taken from the global phenomenological parameters set CH89 proposed in Ref. [31]. The OMP for d+$^{A-1}$C were taken from the parameters set proposed in Ref. [32]. The calculated results of σ_{tra} for the relevant levels are shown in Table 1. σ_{R} for ^{19}C, ^{20}C and ^{22}C with a proton target at low energy (~40 A MeV) have been successfully analyzed by the Galuber model analysis [9,10]. Thus, even for the analysis of the neutron removal cross sections, it is expected that the Glauber model analysis works well. We calculated σ_{diff} by using the few-body Glauber model [33]. In this calculation, the density distributions of the core nucleus and the target nucleus, the wave functions for the valence single neutron, and the finite range parameter were necessary. The density distributions of the core nuclei were assumed to be Harmonic Oscillator type distributions. Parameters of the density distributions of the core nuclei were determined to reproduce the observed σ_{I} with the C target at around 960 A MeV (1104±15 mb for ^{18}C and 1231±28 mb for ^{19}C [3]). Since the target is proton, the density distribution of the target is not necessary. To reproduce observed σ_{R} for p+^{12}C at 40 A MeV (371±11 mb [34]), we determined the finite range parameter. The wave functions of the valence neutron were calculated by solving the eigenvalue problem in a Woods-Saxon potential. The effective separation energy of the valence neutron was reproduced by adjusting the potential depth. In the calculation, the diffuseness and the radius parameter for the potential were fixed to be 0.69 fm and $1.17A^{1/3}$ fm. For the relevant levels, σ_{diff} are given by the difference between the two reaction cross sections, $\sigma_{\mathrm{R}}(^{A}\mathrm{C}+\mathrm{p})$-$\sigma_{\mathrm{R}}(^{A-1}\mathrm{C}+\mathrm{p})$, as summarized in Table 1. The theoretical $\sigma_{-1\mathrm{n}}$ for the each relevant levels was calculated by using Eq. (1). Since, experimentally, inclusive cross sections were measured, we simply summed the theoretical $\sigma_{-1\mathrm{n}}$ of the relevant levels below the one neutron separation energy ($S_{1\mathrm{n}}$) in the A-1 system. $S_{1\mathrm{n}}$ was calculated by the most recent mass evaluation [35]. For the (^{19}C, ^{18}C) reaction, the theoretical inclusive $\sigma_{-1\mathrm{n}}$ is consistent with the observed $\sigma_{-1\mathrm{n}}$. This consistency is also shown in the reaction with the Be target [13]. However, for the (^{20}C, ^{19}C) reaction, the theoretical inclusive $\sigma_{-1\mathrm{n}}$ is larger than the observed $\sigma_{-1\mathrm{n}}$ by the factor of five.

The theoretical $p_{//}$ was calculated by using a CDCC analysis. In the CDCC analysis, elastic breakups with nuclear and Coulomb interactions are taken into account. Here, the cross section of the breakup reaction a(b+X)+A→b+x+A is considered. In the laboratory system, the triple differential cross section (the energy spectrum of the emitted nuclei b) is expressed by [36]

$$\frac{d^3\sigma}{d\Omega_{\mathrm{b}}^{L} d\Omega_{\mathrm{x}}^{L} dE_{\mathrm{b}}^{L}} = \frac{2\pi}{\hbar} \frac{\mu_R}{P_0} \left|T_{\mathrm{fi}}\right|^2 \rho(E_{\mathrm{b}}^{L}) \qquad (2)$$

where Ω_b^L and Ω_x^L represent the direction of emission of b and x respectively, E_b^L is the energy of b in the laboratory frame, μ_R being the reduced mass for a and A. T_{fi} is the transition matrix element and ρ is the phase space factor :

$$\rho(E_b^L) = h^{-6} \frac{m_b m_x m_A P_b P_x}{(m_x + m_A) + \frac{m_x (\boldsymbol{P}_b - \boldsymbol{P}_{tot}^L) \cdot \boldsymbol{P}_x}{P_x^2}} \tag{3}$$

where m_b, m_x, and m_A are mass of b, x and A, respectively, and $\boldsymbol{P}_{tot}^L$ is the total momentum of the system in the laboratory frame. It should be noted that, in Eq. (3), independent variables are $\hat{\boldsymbol{P}}_b(=\Omega_b^L)$, $\hat{\boldsymbol{P}}_x(=\Omega_x^L)$ and $P_b(=\sqrt{2m_b E_b^L})$, and that $\boldsymbol{P}_{tot}^L$ is a constant of motion and $\boldsymbol{P}_x$ is given in terms of those variables and $\boldsymbol{P}_{tot}^L$. The T-matrix element T_{fi} can be expressed in terms of the continuous S-matrix element $S_{lL}^J(k)$ obtained by CDCC:

$$T_{fi} = i\frac{(2\pi\hbar)^3}{\mu_R\sqrt{2}} \frac{1}{k\sqrt{PP_0}} \sum_{lLJM} \sqrt{2J+1} \left[Y_l(\hat{\boldsymbol{k}}) \otimes Y_L(\hat{\boldsymbol{P}})\right]_{JM} e^{i(\delta_{lk}+\sigma_{lk}+\sigma_{L_0}+\sigma_L)} S_{lL}^J(k) \tag{4}$$

where δ_{lk} and σ_{lk} are the nuclear and Coulomb phase shifts of the scattering between b and x, respectively. Transforming ($\hat{\boldsymbol{P}}_b$, $\hat{\boldsymbol{P}}_x$, E_b^L) to ($\hat{\boldsymbol{k}}$, $\hat{\boldsymbol{P}}$, k) in T_{fi}, we can calculate Eq. (2) using the laboratory-frame variables. $p_{//}$ for b is obtained by integrating the triple differential cross section over all solid angle of x and the finite solid angle for b. We used HCTAK [20] for the CDCC analysis. In this calculation, we needed to assume a core-plus-neutron structure for ^{19}C and ^{20}C. The OMP between the valence neutron and the proton target, and the OMP between the core nucleus (^{18}C in ^{19}C and ^{19}C in ^{20}C) and the proton target, have been given by those proposed in Ref. [37], that can be used for the nucleon scattering of 1p-shell nuclei between 10 and 50 MeV. We used the original parameters of the OMP for the (^{19}C, ^{18}C) reaction since σ_R calculated by HCTAK is consistent with the observed one (754±22 mb in [9]). To reproduce the observed σ_R for ^{20}C (791±34 mb in [9]), we adjusted an imaginary radius of the original OMP for ^{20}C. The wave function of the valence neutron was calculated by solving the eigenvalue problem in the Woods-Saxon potential. The effective separation energy of the valence neutron was reproduced by adjusting the potential depth. In the calculation, the diffuseness and the radius parameter for the potential were fixed to be 0.69 fm and $1.17A^{1/3}$ fm. It is noted that in this calculation any bound states were ignored, although the HCTAK calculations allow to include some bound states as well as the ground state. By the above procedure, we calculated $p_{//}$ for the relevant levels, where we assumed the each relevant levels as the ground state. The amplitude of the calculated $p_{//}$ was normalized to the theoretical σ_{1n} of the each relevant levels. The calculated $p_{//}$ with the proton target for the levels below the threshold were summed, as shown in Fig. 3-(b) for the (^{19}C, ^{18}C) reaction and Fig. 4-(a) for the (^{20}C, ^{19}C) reaction, respectively. The summed $p_{//}$ for the (^{19}C, ^{18}C) reaction well reproduces the observed $p_{//}$, as shown in Fig. 3-(a). For the (^{20}C, ^{19}C) reaction, the shape of the observed momentum distributions can be well reproduced by the theoretical distribution, although the theoretical amplitude is much larger than the observed one, as shown in Fig. 4-(a). This result, together with small σ_{1n} for the (^{20}C, ^{19}C) reaction, may indicate that the ground state of ^{20}C has complicated components than a simple ^{19}C core plus one neutron structure.

3-2. Two neutron removal reactions

For the two neutron removal reactions, direct and indirect (one-neutron removal followed by one neutron evaporation) two-neutron removal processes should be taken into account. We considered p(^{20}C, ^{18}C)t reaction as the direct process. Total reaction cross section of the transfer reaction (σ_{tra}) was also calculated by using DWUCK4. The OMP of p+^{20}C was taken from CH89. The OMP of t+^{12}C proposed for the ^{14}C(p, t)^{12}C reaction at E_p=40.3 MeV [38] was simply used as the OMP of t+^{18}C. It is known that the cross sections calculated by DWBA is always much smaller than the experimental data in the (p, t) reactions. We estimated the enhancement factor as follows. We calculated angular distributions for the ^{14}C(p, t)^{12}C reaction leading to the ground state in ^{12}C at E_p=40.3 MeV by using DWUCK4 with the OMP proposed in Ref. [38]. By comparing the calculated results with the experimental data at around 0° shown in Ref. [38], we obtained the enhancement factor (~2000 in this case). We used this enhancement factor to evaluate the total cross section for the p(^{20}C, ^{18}C)t reaction at 40 *A* MeV. The calculated cross sections of the reaction for the relevant levels of ^{18}C are shown in Table 2. The sum of the cross sections for the relevant levels was 4.3 mb. It is noted that the cross section is not sensitive to the choice of the OMP. If we use the OMP from the global phenomenological parameters set GDP08 [39] for t+^{18}C, the cross section of the p(^{20}C, ^{18}C)t reaction for the ground state of ^{18}C was 2.9 mb, where the same enhancement factor was used. Next, we evaluated the indirect process, as follows. If there are levels between the S_{1n} and S_{2n} in the A-1 system, which corresponds to the energy interval between S_{2n} and S_{3n} in the A system, and the neutron single-particle strength between this (neutron unbound) energy interval, the process via one-neutron removal for ^{A}C will contribute to the indirect process. One neutron removal cross sections can be estimated by Eq. (1). In Eq. (1), we considered only $\sigma_{\rm diff}$ for $\sigma_{\rm sp}$. We estimated $\sigma_{\rm diff}$ by using the same procedure described in Sec. 3-1. Here, we calculated $\sigma_{\rm diff}$ for the relevant levels between S_{1n} and S_{2n} in the A-1 system. S_{1n} and S_{2n} were calculated from the recent mass evaluation [35]. By putting the calculated $\sigma_{\rm diff}$ in Eq. (1), we calculated σ_{-1n} for the relevant levels. Since the observed σ_{-2n} is inclusive, we summed the calculated σ_{-1n} of the relevant levels between S_{1n} and S_{2n} in the A-1 system, and assumed the sum as the theoretical inclusive indirect σ_{-2n}, as shown in Table 1. The sum (14.7 mb) of the direct process (4.3 mb) and the indirect process (10.4 mb) is much smaller than the observed σ_{-2n} by the factor of six.

For the calculations of $p_{//}$, we used HCTAK. Procedure of the calculation is the same as that described in Sec. 3-1. Here, we took into account only indirect process. In the indirect process, we assumed the shape of the momentum distributions does not change even after the sequential one-neutron evaporation. We summed the momentum distributions for the four states (E_x=0.62 MeV to E_x=3.72 MeV shown in Table 1), and showed only the sum in Fig. 4-(b). Although the amplitude of the theoretical distribution is much smaller than the observed one, the shape of the theoretical distribution can well reproduce the shape of the observed distribution.

It is noted that discrepancy between the theoretical and the observed removal cross sections is opposite between one and two neutron removal reactions from ^{20}C. In the (^{20}C, ^{19}C) reaction, the theoretical cross section is much larger than the observed one. On the other hand, in the (^{20}C, ^{18}C) reaction, the theoretical cross section is much smaller than the observed one. For the (^{20}C, ^{19}C) reaction, our shell model calculation shows that the energies of the three levels (E_x=0 MeV, 0.19 MeV and 0.62 MeV) are very close. If the effective interaction changes a little, the order of the levels would be changed. For example, if the order of the level with E_x=0.19 MeV and that with E_x=0.62 MeV swaps and the first $5/2^+$ state becomes unbound, theoretical cross sections will approach to the experimental ones. In Ref. [40], two γ-rays with 72±4 and 197±6 keV have been observed in ^{19}C. On the other hand, in Ref. [41], only one γ-ray with 201±15 keV has been observed in ^{19}C. Thus, at least two bound states exist in ^{19}C. Thus, if the first $5/2^+$ state is unbound, the two bound states must be $1/2^+$ and $3/2^+$ and there only one γ-ray should be observed. In Ref. [42], an excited state at 1.46±0.19 MeV in ^{19}C populated in the inelastic proton scattering was observed to the neutron decay. This state may correspond to the second $5/2^+$ (E_x = 1.54 MeV in Table 1) in our shell model calculations. The calculated B(E2) to the second $5/2^+$ state is six times larger than to the first $5/2^+$ state. Thus, if the first $5/2^+$ state is unbound, it may be located just above the neutron decay threshold and decay by a low-energy neutron that may have been too weak to observe in Ref. [42]. For the conclusive statements for the excited states in ^{19}C, further experimental and theoretical investigations are needed.

In the present analysis, we assumed the peripheral reactions with the proton target. This assumption might be valid for ^{19}C, where the one neutron halo structure is dominated in the ground state. However, for ^{20}C, central collisions may contribute to the dominant part of the neutron removal cross sections specially for the (^{20}C, ^{18}C) reaction. Theoretical descriptions including the central collisions with the proton target are anticipated.

4. Summary

One and two-neutron removal reactions from ^{19}C and ^{20}C have been studied using a liquid-hydrogen target at 40 A MeV. The longitudinal momentum distribution ($p_{//}$) of the (^{19}C, ^{18}C) reaction is broader than that previously measured with a Be target. A broad $p_{//}$ with a small cross section has been observed in the (^{20}C, ^{19}C) reaction. We calculated theoretical cross sections for one neutron removal reactions by using the shell model spectroscopic factors and the single particle cross sections using Glauber model. We applied CDCC calculations to interpret $p_{//}$. For the (^{19}C, ^{18}C) reaction, the calculated results for the inclusive σ_{-1n} and $p_{//}$ can well reproduce the observed cross sections and $p_{//}$. On the other hand, for the (^{20}C, ^{19}C) reaction, our calculations overestimated the observed σ_{-1n} although the shape of $p_{//}$ is consistent with the observed $p_{//}$. For the (^{20}C, ^{18}C) reaction, although the shape of theoretical $p_{//}$ is consistent with the observed one, the observed σ_{-2n} is much larger than theoretical σ_{-2n}. These discrepancies may suggest that the first $5/2^+$ state in ^{19}C, which is bound in our shell model calculations, may not be bound. For the conclusive statements, further experimental investigations and improvements of the theoretical descriptions are necessary. Theoretical descriptions including the central collisions with the proton target are also anticipated.

Acknowledgements

The authors thank the members of the RIKEN accelerator staff for stable operation of the accelerators and related devices. We thank Professor J. Tostevin for providing the shell model calculations.

References

[1] I. Tanihata, J. Phys. G 22 (1996) 157.
[2] T. Suzuki et al., Phys. Rev. Lett. 89 (2002) 012501.
[3] A. Ozawa et al., Nucl. Phys. A 691 (2001) 599.
[4] E. Sauvan et al., Phys. Rev. C 69 (2004) 044603.
[5] T. Yamaguchi et al., Nucl. Phys. A 724 (2003) 3.
[6] M. Chiba et al., Nucl. Phys. A 741 (2004) 29.
[7] D.Q. Fang et al., Phys. Rev. C 69 (2004) 034613.
[8] A. Ozawa et al., Phys. Rev. C 78 (2008) 054313.
[9] K. Tanaka et al., Phys. Rev. Lett. 104 (2010) 062701.
[10] T. Yamaguchi et al., Nucl. Phys. A in press.
[11] W. Horiuchi and Y. Suzuki, Phys. Rev. C 74 (2006) 034311.
[12] B. Abu-Ibrahim et al., Phys. Rev. C 77 (2008) 034607.
[13] E.C. Simpson and J.A. Tostevin, Phys. Rev. C 79 (2009) 024616.
[14] M. Stanoiu et al., Phys. Rev. C 69 (2004) 034312.
[15] A. Schiller et al., Phys. Rev. Lett. 99 (2007) 112501.
[16] M. Stanoiu et al., Phys. Rev. C 78 (2008) 034315.
[17] Z. Elekes et al., Phys. Rev. C 79 (2009) 011302(R).
[18] Y. Kondo et al., Phys. Rev. C 79 (2009) 014602.
[19] M. Yahiro et al., Prog. Theor. Phys. Suppl. 89 (1986) 32.
[20] Y. Aoki et al., RIKEN Accel. Prog. Report 2009, 43 (2010) 22.
[21] T. Kubo et al., Nucl. Instrum. Methods B 70 (1992) 309.
[22] H. Kumagai et al., Nucl. Instrum. Methods A 470 (2001) 562.
[23] H. Ryuto et al., Nucl. Instrum. Methods A 555 (2005) 1.
[24] S. Takeuchi et al., RIKEN Rev. 36 (2003) 148.
[25] K. Kusaka, et al., IEEE Trans. Appl. Supercond. 14 (2004) 310.
[26] S. Takeuchi et al., Phys. Rev. C 79 (2009) 054319.
[27] N. Iwasa et al., Nucl. Instrum. Methods B 126 (1997) 284.
[28] B.A. Brown et al., computer program OXBASH for Windows (2004), MSU-NSCL

Rep. No. 1289 (unpublished).

[29] E.K. Warburton and B.A. Brown, Phys. Rev. C 46 (1992) 923.

[30] P.D. Kuntz, computer program DWUCK4 (unpublished).

[31] R. L. Varner et al., Phys. Rep. 201 (1991) 57.

[32] W.W. Daehnick et al., Phys. Rev. C 21 (1980) 2253.

[33] Y. Ogawa et al., Nicl. Phys. A 571 (1994) 784.

[34] R.F. Carlson, Atomic Data and Nucl. Data Tables 63 (1996) 93.

[35] G. Audi et al., Nucl. Phys. A 729 (2003) 337.

[36] Y. Iseri et al., Prog. Theor. Phys. Suppl. 89 (1986) 84.

[37] B.A. Watson et al., Phys. Rev. 182 (1969) 977.

[38] M. Yasue et al., Nucl. Phys. A 510 (1990) 285.

[39] D.Y. Pang et al., Phys. Rev. C 79 (2009) 024615.

[40] Z. Elekes et al., Phys. Lett. B 614 (2005) 174.

[41] M. Stanoiu et al., Eur. Phys. J. A 20 (2004) 95.

[42] Y. Satou et al., Phys. Lett. B 660 (2008) 320.

Reaction	E_x(MeV)	J^π	l	σ_{tra}(mb)	σ_{dif}(mb)	C^2S	σ_{-1n}(mb)	σ_{exp}(mb)
(^{19}C,^{18}C)	0.00	0+	0	1.7	93.4	0.580	61.5	
S_{1n}=4.18MeV	2.14	2+	2	6.4	21.9	0.470	14.8	
	3.64	2+	2	7.4	18.3	0.104	3.0	
	3.99	0+	0	9.0	31.3	0.319	14.3	
		Inclusive					93.6	101±11
(^{20}C,^{19}C)	0.0	1/2+	0	8.5	33.8	1.099	51.5	
S_{1n}=0.58MeV	0.19	5/2+	2	4.5	15.1	3.649	75.3	
S_{2n}=4.76		Inclusive					126.8	22±8
	0.62	3/2+	2		14.0	0.247	3.6	
	1.54	5/2+	2		12.3	0.282	3.7	
	3.28	3/2+	2		9.9	0.191	2.0	
	3.72	1/2+	0		18.7	0.055	1.1	
		Inclusive (indirect 2n removal)					10.4	

Table 1. Results for one-neutron removal reactions from ^{19}C (^{20}C) to bound (and unbound) final states of ^{18}C (^{19}C), respectively. E_x means the excited energy in A-1 system, i.e., ^{18}C (^{19}C) for the (^{19}C, ^{18}C) reaction (the (^{20}C, ^{19}C) reaction), respectively. The calculations are for a proton target at 40 A MeV. σ_{-1n} include the center-of-mass correction factor $[A/(A-1)]^N$. Neutron separation energies (S_{1n} and S_{2n}) for A-1 system were calculated by the recent mass evaluation [35]. Levels with $0.58<E_x<4.76$ MeV in ^{19}C contribute to the indirect two-neutron removal in ^{20}C.

Reaction	E_x(MeV)	σ_{tra}(mb)
(^{20}C, ^{18}C)	0	2.2
S_{1n}=4.18MeV	2.14	0.5
	3.64	0.4
	3.99	1.2
Inclusive (direct 2n removal)		4.3

Table 2. Results of the calculated cross sections of the p(^{20}C, ^{18}C)t reaction at 40 *A* MeV for the relevant levels of ^{18}C. The calculations were done using DWUCK4 [30] with the OMP proposed in Ref. [38] for t+^{18}C. In the calculations, phenomenological enhancement factor (~2000) was taken into account. E_x means the excited energy in ^{18}C.

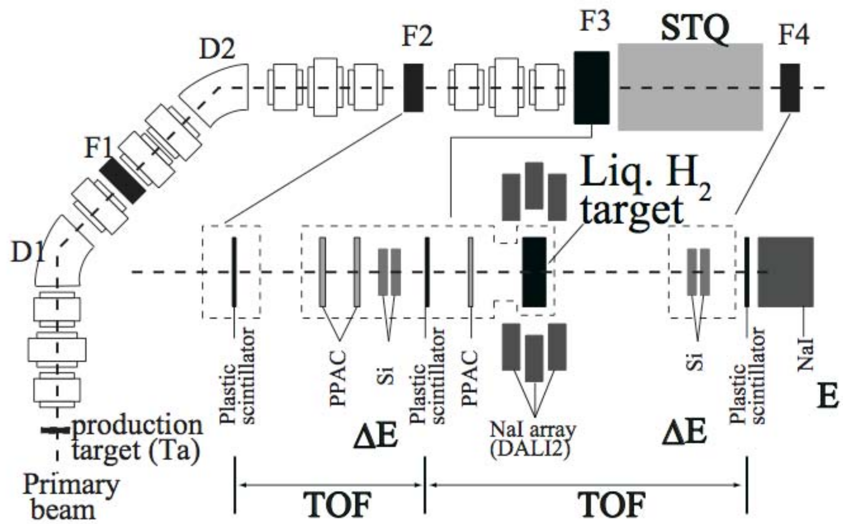

Fig.1 Schematic drawing of the experimental setup in RIPS [21].

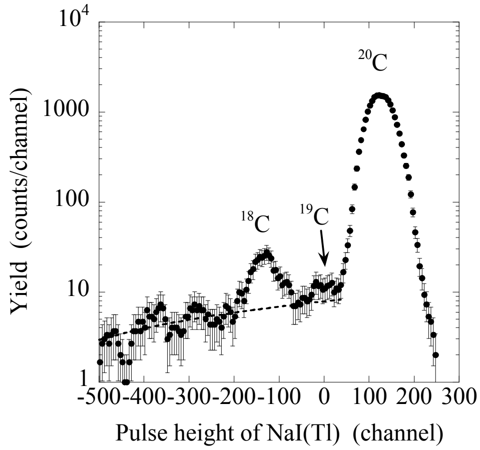

Fig. 2. Typical mass spectrum in ^{20}C break-up. Here, Z=6 was selected by ΔE in the Si detectors at F4. The energy spectrum measured in NaI(Tl) was corrected by TOF between F3 and F4. A broken line shows the ^{20}C reaction events inside NaI(Tl).

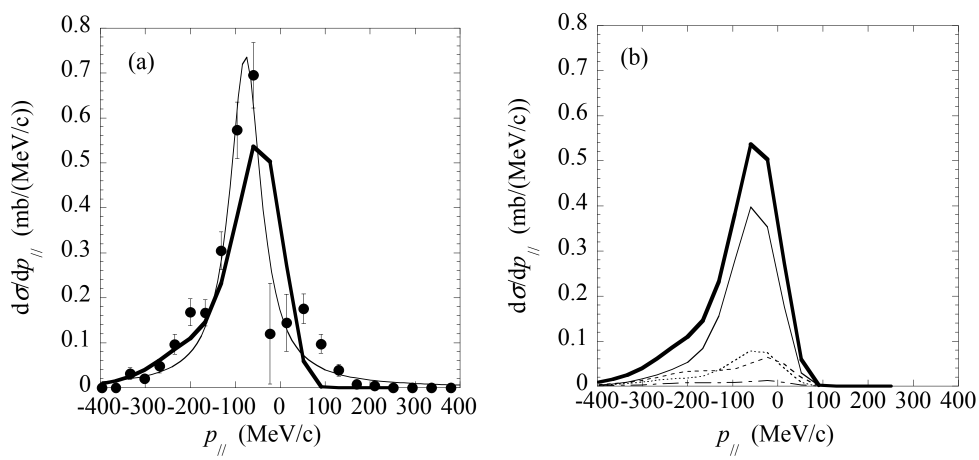

Fig. 3. (a) Fragment longitudinal momentum distributions ($p_{//}$) for the (^{19}C, ^{18}C) reaction with a hydrogen target at 40 A MeV. Closed circles are experimental data, while a thin solid line is a fitted result by the Lorentzian function. The thick solid line shows the summed theoretical $p_{//}$ calculated by our CDCC. (b) Theoretical $p_{//}$ for the (^{19}C, ^{18}C) reaction with a proton target at 40 A MeV. $p_{//}$ for E_x=0.0 MeV in Table 1 is shown by a thin solid line. $p_{//}$ for E_x=2.14 MeV, 3.64 MeV and 3.99 MeV are shown by broken, dashed and dotted lines, respectively. A thick solid line shows the sum of the four $p_{//}$.

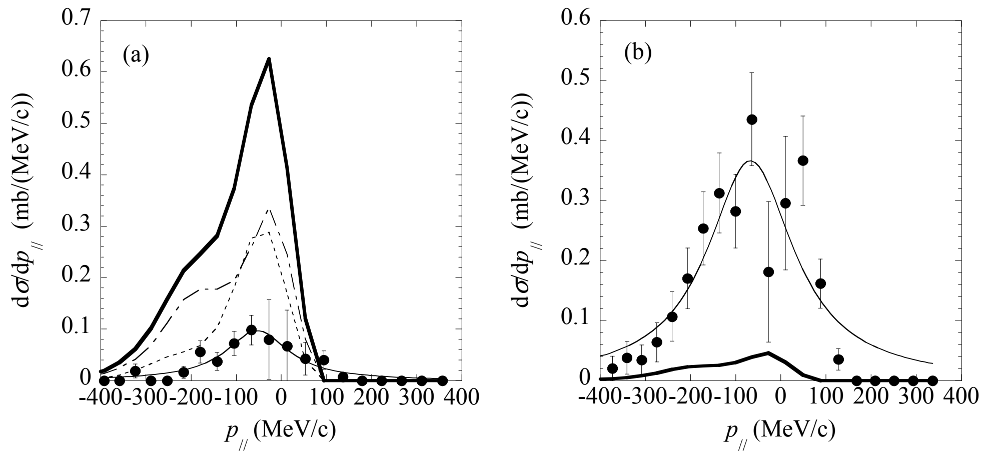

Fig. 4. (a) Fragment longitudinal momentum distributions ($p_{//}$) for the (^{20}C, ^{19}C) reaction with a hydrogen target at 40 *A* MeV. Closed circles are experimental data, while a thin solid line is a fitted result by the Lorentzian function. Broken and dashed lines show the theoretical $p_{//}$ for E_x=0.0 MeV and E_x=0.19 MeV, respectively. A thick solid line shows the sum of the two $p_{//}$. (b) Fragment longitudinal momentum distributions ($p_{//}$) for the (^{20}C, ^{18}C) reaction with a hydrogen target at 40 *A* MeV. Closed circles are experimental data, while a thin solid line is a fitted result by the Lorentzian function. A thick solid line shows the sum of the four $p_{//}$ (E_x=0.62 MeV, 1.54 MeV, 3.28 MeV and 3.72 MeV in Table 1).